Hydrometallurgy 211 (2022) 105864

Contents lists available at ScienceDirect

Hydrometallurgy

journal homepage: www.elsevier.com/locate/hydromet

Beneficial effect of iron oxide/hydroxide minerals on sulfuric acid baking and leaching of monazite

John Demol [a,b], Elizabeth Ho [a,*], Karin Soldenhoff [a], Inna Karatchevtseva [a], Gamini Senanayake [b,*]

[a] Australian Nuclear Science and Technology Organisation (ANSTO), New Illawarra Rd, Lucas Heights, New South Wales 2234, Australia
[b] College of Science, Health, Engineering and Education, Murdoch University, 90 South Street, Murdoch, Perth, WA 6150, Australia

ARTICLE INFO

Keywords:
Monazite
Rare earth
Thorium
Acid bake
Sulfation
Goethite
Hematite
Magnetite

ABSTRACT

The sulfuric acid bake/leach process is an established industrial process for the extraction of rare earths from hard-rock monazite ores/concentrates. The chemical reactions in the monazite acid bake can be strongly influenced by the gangue mineralogy of the ore/concentrate. In this work, the beneficial effect of three iron oxide/hydroxide minerals, namely hematite, goethite and magnetite, added to high grade monazite concentrate in the acid bake (temperature range of 200–800°) and leach process was investigated to understand the role of iron gangue. Baked solids and leach residues were characterised by elemental analyses, XRD, SEM-EDS and FT-IR. It was found that the addition of iron minerals to the monazite acid bake had a significant impact on bake chemistry, acting to significantly increase the leaching of both the rare earth elements and thorium, compared to monazite alone, mainly for temperatures above 300 °C. The increased dissolution of rare earth elements and thorium was attributed to the formation of an amorphous and insoluble iron sulfate-polyphosphate type phase in preference to insoluble rare earth and thorium containing polyphosphates identified during acid baking of monazite alone. After baking at 650 °C, the iron sulfate-polyphosphate type phase was altered to a more soluble form, leading to an increase in dissolution of iron, phosphorus and thorium. Acid baking at 800 °C led to the formation of $FePO_4$, Fe_2O_3, $CePO_4$ (monazite) and in some cases CeO_2, causing a decrease in leaching of rare earths and thorium, and either an increase or a decrease in leaching of iron and phosphorus depending on the formation of $FePO_4$ versus Fe_2O_3.

1. Introduction

Rare earth elements are used in numerous high-tech applications spanning the renewable energy, defence and industry sectors. One of the major sources of rare earth elements is monazite, a rare earth and thorium phosphate mineral with formula $(Ln,Th)PO_4$ (Castor and Hedrick, 2006). Monazite is found in both placer deposits and hard-rock deposits. Hard-rock deposits are mainly classified as carbonatite-associated, including weathered carbonatite, and vein deposits (Castor and Hedrick, 2006; Wall, 2014). Hard-rock rare earth ores generally have a complex mineralogy, containing a significant proportion of gangue minerals, such that rare earth element concentrations are typically in the 5–15% (*w*/w) range (Lucas et al., 2015). Complete removal of gangue minerals via beneficiation is usually difficult.

The major industrial process currently used for processing of monazite bearing ores/concentrates is the sulfuric acid bake, which, for example, is used at Bayan Obo in China, for processing of Baotou mixed bastnasite/monazite concentrate, and for processing monazite concentrate from Mt. Weld in Australia (Lucas et al., 2015; Lynas Corporation Ltd, 2011; Zhang et al., 2015). Gangue minerals in a monazite concentrate/ore can potentially have a significant impact on the acid bake process but there have been relatively few studies in the literature focused on examining the effects of gangue minerals during acid baking. Given the significance of the acid bake in the global rare earth industry, there is a need for improving the fundamental understanding of the way gangue minerals affect monazite reactions in the acid bake and through this, the extraction of rare earth elements and impurities in the subsequent water/acid leaching step.

One group of gangue minerals well represented in hard-rock monazite bearing ores is the iron oxide/hydroxide mineral group, which includes minerals such as hematite (Fe_2O_3), goethite (FeOOH) and magnetite (Fe_3O_4). These minerals also undergo acid baking reactions

* Corresponding authors.
E-mail addresses: eho@ansto.gov.au (E. Ho), G.Senanayake@murdoch.edu.au (G. Senanayake).

https://doi.org/10.1016/j.hydromet.2022.105864
Received 21 September 2021; Received in revised form 17 February 2022; Accepted 22 March 2022
Available online 26 March 2022

and affect the performance of monazite. Gontijo et al. (2020) studied the sulfation reactions of three hematite samples, goethite and magnetite during acid baking in the temperature range of 80–240 °C. Iron dissolution in the leaching stage increased in the order of goethite >> magnetite > hematite and the varying reactivities in the acid bake/leach were attributed to differing mineral porosities, specific surface area and crystalline structure. The extent of reaction of the iron oxide minerals was limited by the formation of a ferric sulfate product layer.

Other studies examined higher bake temperatures. Wang et al. (2010) conducted a thermal analysis study of the acid baking of the mixed bastnasite/monazite Baotou concentrate from China, which contains iron oxide minerals (2.5% *w*/w Fe). Published reactions show hematite reacting to form ferric sulfate at 150–250 °C, before decomposing to re-form hematite at temperatures above 425 °C (Wang et al., 2010). The hematite re-formation caused the iron dissolution to decrease. Interestingly, thermogravimetric studies of pure ferric sulfate show the decomposition to hematite occurring in the higher temperature range of 500 to 700 °C (Mu and Perlmutter, 1981; Tagawa, 1984).

Some studies also report the formation of iron phosphates during acid baking at higher temperatures (>300 °C). In a patent related to acid baking, Li et al. (2009) describes a process where a hematite bearing monazite ore is acid baked at 231–600 °C. Ferric sulfate, formed from the initial reaction with acid, is claimed to react with pyrophosphoric acid ($H_4P_2O_7$) at 300 °C to form insoluble iron pyrophosphate ($Fe_4(P_2O_7)_3$). The pyrophosphoric acid is reportedly formed from the dehydration of orthophosphoric acid (H_3PO_4), which is a product of the initial reaction of monazite with sulfuric acid. In another patent, Teixeira and Silva (2015) also propose the formation of an iron phosphate during acid baking of an iron-rich monazite ore at a higher temperature of 650–750 °C, albeit via a different mechanism. The proposed chemical reactions show ferric sulfate reacting with phosphoric acid or monazite to give iron orthophosphate ($FePO_4$). Yoon et al. (2015) found that a $NdFeO_3$ phase formed at 600 °C from Nd_2O_3 and Fe_2O_3, in a study examining the air roasting of neodymium-iron-boron magnet scraps following treatment with sodium hydroxide. The incorporation of neodymium into the iron oxide resulted in a decrease in the dissolution of neodymium relative to roasting at lower temperatures (<500 °C). Although the studies summarised above suggest that iron minerals associated with monazite participate in various chemical reactions in the acid bake process, no study to date has systematically examined these effects in light of their impact on the dissolution of rare earth elements and impurities during subsequent water leaching.

The objective of this study was to investigate acid baking of monazite with iron minerals in the temperature range of 200–800 °C and their impact on subsequent ambient temperature acid (pH ≤ 1) leaching of rare earths, thorium, phosphate and iron from the baked solids. The acid baking of each iron mineral was studied as a mixture with high grade, iron free, monazite concentrate. Characterisation of solid reaction products formed in the acid bake and after leaching was by elemental analyses, XRD, SEM-EDS and FT-IR. Thermodynamic modelling of bake products using the HSC software package using the existing data base (Appendix A) as well as thermogravimetric analyses (TG-DSC) of monazite with acid and iron minerals were also carried out to shed more light on the effect of iron minerals on bake/leach chemistry.

2. Materials and methods

The monazite sample was a mineral sands concentrate from an Australian placer deposit and contained no iron. Natural mineral samples of hematite (Fe_2O_3), goethite (FeOOH) and magnetite (Fe_3O_4) from Australian sources were purchased from a commercial supplier. All samples were crushed and ground in a ring mill prior to acid baking and leaching experiments. A schematic of the acid bake/leach process is given in Fig. 1.

The high-grade monazite concentrate or its 1:1 (*w*/w) mixture with each iron mineral was intimately mixed with concentrated (96% w/w) sulfuric acid using a spatula and placed in a muffle furnace. The sulfuric acid addition was 200% of that required to provide sufficient acid to convert all cations in the sample to sulfate salts. For the acid addition calculations, it was assumed that iron was trivalent in the reaction products formed after baking with monazite (Table 1). For the 200 °C and 250 °C bakes, the sample/acid mixture was placed in a muffle furnace pre-heated to 100 °C, heated to the target temperature at 5 °C/min, held for 2 h, and directly removed from the furnace. For bake temperatures above 250 °C, the samples were first baked at 250 °C for 2 h to ensure complete sulfation of monazite before heating at 5 °C/min to the final target temperature and holding for 2 h. Some acid bakes of individual iron minerals were also carried out to compare iron dissolution to the iron mineral/monazite bakes. For bakes of the individual iron minerals, the sulfuric acid addition was 150% of the acid required to provide sufficient acid to convert all cations in the sample to sulfate salts.

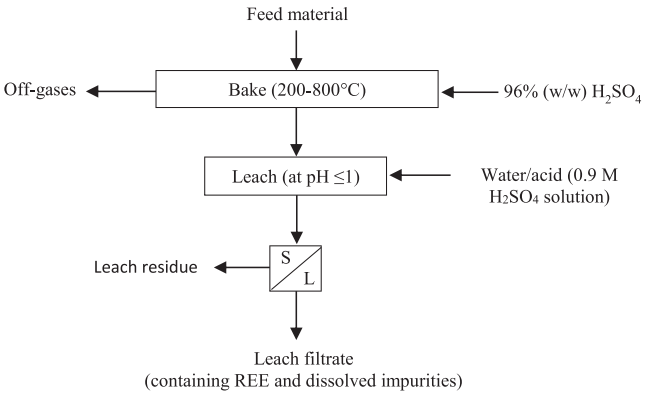

Fig. 1. Schematic of acid bake and leach process.

The baked samples were cooled and ground to a fine powder in a mortar and pestle. The bake product of iron mineral/monazite mixture was leached in 0.9 M sulfuric acid at a liquid to solid ratio (*w*/w) of 40:1 (monazite alone and mixtures) at 20–25 °C for 2 h, unless otherwise stated.

Slurry samples collected after leaching were filtered and the clarified leach solutions were analysed by inductively-coupled plasma optical emission spectroscopy (ICP-OES) as well as inductively-coupled plasma mass spectrometry (ICP-MS). Bake solids and leach residues were characterised by a combination of x-ray fluorescence spectroscopy (XRF), x-ray diffraction (XRD), scanning electron microscopy with energy dispersive spectroscopy (SEM-EDS) and Fourier-transform infrared spectroscopy (FT-IR) using the same instrumentation and methodology as previously described in Demol et al. (2018). Elemental mass balances were calculated to ensure reliability of the reported elemental extractions. Bake solids and leach residues were examined by SEM-EDS to characterise the amorphous reaction products formed in the bake process. Bake solids produced at temperatures of ≤300 °C were moist due to excess sulfuric acid and were washed with acetone to remove the acid

Table 1
Summary of acid additions used for iron mineral/monazite concentrate acid bake tests.

Feed mixtures* to acid bake	Acid addition	
	(% stoichiometric**)	(kg/t)
Hematite/Monazite	200	2200
Goethite/Monazite	200	2200
Magnetite/Monazite	200	1800

* Mixtures were 1:1 (w/w).
** Stoichiometric is defined here as the amount of acid required to provide sufficient sulfate ions to react with all cations in the sample, irrespective of the degree of reaction.

prior to mounting for XRD analysis. Deconvolution of the FT-IR spectra was carried out using the built-in OMNIC software package. The mineral phases in the monazite and iron mineral samples were analysed using QEMSCAN (quantitative evaluation of minerals by scanning electron microscopy), an automated mineral analysis software using SEM-EDS, in addition to the above techniques. The TG-DSC analyses of mineral/acid mixtures were carried out using a TA Instruments SDT-Q600. Particle size distributions were measured by laser sizing using a Malvern Mastersizer.

3. Results and discussion

3.1. Chemical analyses and mineralogical characterisation of samples

Elemental compositions of the three iron mineral samples and the monazite sample are provided in Table 2 and Table 3, respectively. The iron mineral samples contained mainly Fe with significant Si content in the goethite and hematite samples and Al content in the goethite sample. Characterisation of the monazite sample has been previously reported (Demol et al., 2018). Monazite was the major component (93% *w*/w), with a small amount of zircon (5% w/w) also present and the remainder made up of trace minerals. The monazite concentrate contained 50% (*w*/w) total rare earths (TRE) as shown in Table 3, in the descending order of Ce > La > Nd > Pr.

Results from QEMSCAN and XRD analyses of the iron mineral samples are summarised in Table 4 and Table 5, respectively. Specific iron oxide/hydroxide minerals cannot be differentiated by SEM-EDS, due to the similarity in elemental composition. The hematite sample contained 85% (*w*/w) iron oxide/hydroxide mineral(s) and 11% (w/w) quartz. The XRD analysis confirmed that the iron mineral was hematite. The goethite sample contained quartz (Table 5). The elemental composition was equivalent to a goethite content of 62% (*w*/w) and a quartz content of 24% (w/w). The magnetite sample was mainly composed of a mixture of two iron oxides, making up 98% (w/w) of the sample (Table 4). The XRD analysis showed the presence of predominantly magnetite and hematite.

The particle size distributions for the monazite and iron mineral samples after milling are presented in Table 6. The same milled hematite and magnetite samples were used for bakes of iron mineral/monazite/H_2SO_4 mixtures and iron mineral/H_2SO_4 mixtures. Additional goethite sample was milled for the mixed goethite/monazite bakes and this had a finer particle size distribution than the sample used for the goethite only bakes. The same milled monazite sample was used for all bakes.

3.2. Acid baking and leaching of monazite/iron mineral mixtures

3.2.1. Effect of baking with iron minerals on leaching

(a) *Effect on leaching of rare earths*

Fig. 2 shows the effect of each iron mineral on rare earth dissolution, after acid baking at a ratio of 1:1 (*w*/w) with monazite in the temperature range of 200–800 °C and leaching in 0.9 M H_2SO_4 at a liquid to solid ratio of 40:1 (*w*/w) as depicted in Fig. 1. Acid, rather than water, was used for leaching the baked solids to avoid exceeding the potential solubility limits for thorium phosphates. The data for acid baking of monazite alone in Fig. 2 is from a previous study using similar bake and the same leach conditions (Demol et al., 2018). It is included here for comparison. A typical elemental mass balance for major elements for a bake and leach test, as well as figures showing dissolution of individual light rare earths are provided in Appendix C.

For acid bakes of monazite alone, the rare earth dissolution increased from 91% after a 200 °C bake to 99% after a 300 °C bake. At bake temperatures above 300 °C, the rare earth extraction decreased due to their partial incorporation within an insoluble, amorphous thorium polyphosphate phase of undefined composition, $(Th,RE)(PO_x)_n$ (Demol et al., 2018). It was proposed that the formation of insoluble thorium and rare earth polyphosphates is due to the dehydration of

Table 2
Elemental composition of hematite, goethite and magnetite samples by XRF.

Iron mineral sample	Elemental composition (% w/w)				
	Al	Fe	P	Si	Ti
Hematite	<0.1	63.0	<0.1	4.66	<0.1
Goethite	1.14	39.1	0.43	11.3	0.04
Magnetite	0.49	68.0	<0.1	0.42	0.84

Table 3
Elemental composition of monazite sample[a].

Element	Al	Ca	Ce	La	Nd	P	Pr	S
Mass % (w/w)	0.26	0.69	23.3	12.0	9.2	11.5	2.34	0.02
Element	Si	Th	Ti	Zr	Y	LRE[b]	HRE[c] + Y	TRE
Mass % (w/w)	1.39	5.97	0.20	2.46	0.78	46.8	3.21	50.1

[a] Eu, Ho and Yb were analysed by digest and ICP-MS, which is more reliable than XRF for low concentrations of these elements. All other elements were analysed by XRF.
[b] Light rare earths: La,Ce,Pr,Nd.
[c] Heavy rare earths: Sm-Lu.

Table 4
Components of iron mineral samples by QEMSCAN.

Iron mineral	Component minerals	Formula	Concentration (% w/w)
Hematite	Iron oxides/hydroxides	e.g. Fe_2O_3, Fe_3O_4, or FeO(OH)	87.9
	Quartz	SiO_2	11.5
	Trace minerals	–	0.7[b]
Goethite	Iron oxides/hydroxides	e.g. Fe_2O_3, Fe_3O_4, or FeO(OH)	81.6
	Quartz	SiO_2	11.1
	Jarosite	$KFe_3(SO_4)_2(OH)_6$	3.7
	Chlorites	e.g. $(Fe^{2+},Mg,Fe^{3+})_5Al(Si_3Al)O_{10}(OH,O)_8$[a]	1.6
	Trace minerals	–	2.0[b]
Magnetite	Iron oxides/hydroxides	e.g. Fe_2O_3, Fe_3O_4, or FeO(OH)	97.8
	Trace minerals	–	2.2[b]

[a] Chamosite.
[b] Table 2.

Table 5
Components of iron mineral samples identified by XRD.

Iron mineral	Hematite	Goethite	Magnetite
Components	Fe_2O_3, SiO_2	FeOOH, SiO_2	Fe_3O_4, Fe_2O_3

Table 6
Particle size distributions by volume for iron mineral samples and monazite.

Percent passing (%)	10	20	50	80	90
Hematite (μm)	4.8	17	69	127	160
Goethite[a] (μm)	1.5	4.2	22	111	175
Goethite[b] (μm)	1.2	3.5	14	33	53
Magnetite (μm)	2.6	5.4	25	102	144
Monazite (μm)	1.4	3.5	15	44	76

[a] Goethite sample used in individual goethite bakes;
[b] Goethite sample used in bakes of goethite/monazite mixtures (grinding of additional goethite was required for tests with mixtures).

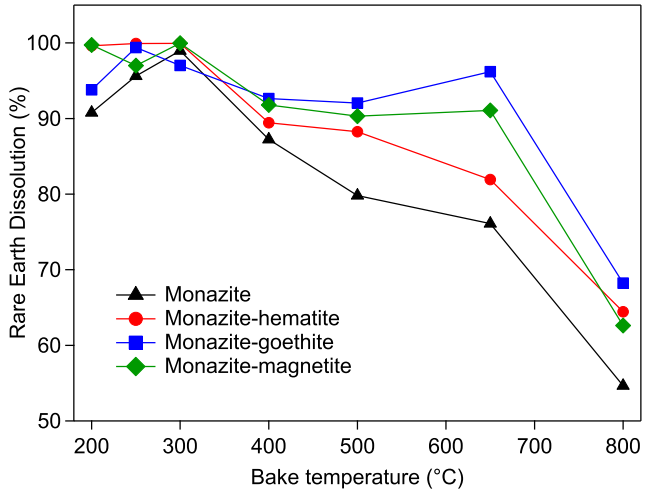

Fig. 2. Effect of iron minerals on total rare earth dissolution after acid baking and leaching iron minerals with monazite (1:1 w/w) compared to monazite alone. (Bake conditions: 250% stoichiometric acid addition for monazite, 200% stoichiometric acid addition for monazite-iron mineral mixtures where stoichiometric is defined as the acid required to react with all cations; Leach conditions: 0.9 M H_2SO_4, liquid to solid ratio of 40:1 (w/w), 2 h, 20–25 °C; data for monazite from Demol et al., 2018).

orthophosphoric acid, formed in the initial sulfation reaction of monazite, to form polyphosphoric acids at temperatures greater than 300 °C.

Fig. 2 indicates different leaching behaviours depending upon the type of iron mineral and the temperature below or above 300 °C. The addition of iron minerals increased the extraction of rare earth elements relative to acid baking of monazite on its own, particularly for bake temperatures greater than 300 °C. The beneficial effect of all three iron minerals at bake temperatures below 300 °C in Fig. 2 may be due to excess sulfuric acid added to react with iron minerals (Table 1), being available for further reaction with monazite. At bake temperatures >300 °C, goethite had the greatest beneficial effect on the rare earth dissolution, increasing the rare earth dissolution from 76% for monazite alone, to 96% in the presence of goethite, for a bake temperature of 650 °C. Hematite had the smallest effect on rare earth dissolution relative to monazite alone, which corresponds to the lower reactivity of hematite in the acid bake, as seen in Section 3.2.1b. The beneficial effect of iron minerals at bake temperatures >300 °C will be revealed in light of mineralogical analyses.

(b) *Effect on leaching of iron*

Iron dissolution from the acid bakes of iron mineral/monazite mixtures and the individual iron mineral samples is compared in Fig. 3. For the iron mineral bakes, leaching was conducted in water at a liquid to solid ratio (*w*/w) of 20:1 and controlled at pH < 1 by addition of concentrated sulfuric acid if required. Although the leach medium after the iron mineral bakes was less acidic than for the monazite/iron mineral bakes, trends can be compared. For bake temperatures <300 °C, the iron dissolution was lower for the mixtures with monazite. In the case of acid bake and water leach of iron mineral samples, the reactivity of hematite was much lower than for goethite and magnetite, in agreement with Gontijo et al. (2020). The slightly larger particle size distribution of the hematite sample (Table 6) would also have slightly decreased the hematite reactivity due to its lower specific surface area. In the 300–500 °C temperature range, the iron dissolution from the bake product of the mixture with monazite decreased sharply (Fig. 3b, c), diverging significantly from the behaviour of the individual iron mineral samples. This indicates the formation of insoluble iron containing phases caused by the presence of monazite.

The dissolution of iron decreased to <1% for bakes of magnetite and hematite individually at 800 °C and to <10% for goethite after baking at 750 °C. This was attributed to the decomposition of iron sulfate produced by the reaction with H_2SO_4 used for baking, to iron oxide via Eq. (1), which is reported to occur between 500 °C and 700 °C (Mu and Perlmutter, 1981; Tagawa, 1984).

$$Fe_2(SO_4)_3 \rightarrow Fe_2O_3 + SO_2(g) + \tfrac{1}{2}O_2(g) \quad (1)$$

After baking the iron mineral/monazite mixtures at 800 °C, the iron dissolution was slightly higher than observed for the individual iron minerals, in all cases (Fig. 3). This indicated that a fraction of iron resided in a phase other than Fe_2O_3 at this temperature when baked with monazite. The phases formed during baking are discussed in more detail in Section 3.3.2.

(c) *Effect on leaching of thorium, phosphorus and sulfur*

The effect of the iron minerals on dissolution of thorium, phosphorus and sulfur are presented in Fig. 4 which shows a strong dependence on bake temperature. Sulfur dissolution was calculated with respect to the solids produced after baking and does not include the sulfur volatilised in the bake. The dissolutions of other elements were calculated with respect to the feed to the bake. For the bakes in the temperature range of 200–250 °C, extractions from the baked iron mineral/monazite mixtures were similar to the results from monazite alone with generally high dissolution of thorium, phosphorus and sulfur. This observation supports the formation of either soluble thorium phosphate or sulfate in the leach medium as revealed by the Eh-pH diagrams (Kim and Osseo-Asare, 2012; Demol et al., 2019).

For acid bakes of monazite alone at temperatures ≥250 °C, extractions of thorium and phosphorus decreased but sulfur dissolution remained at >90% indicating a predominantly soluble form of sulfate in bake products. The presence of iron minerals during baking resulted in a substantial increase in leaching of thorium after baking at the temperature range 300–800 °C. For a bake temperature of 400–500 °C, phosphorus dissolution was <15%. In contrast, the phosphorus dissolution was significantly increased by addition of iron minerals, for bake temperatures of 650 °C and above, implying the formation of soluble phosphate phases. After baking in the presence of iron minerals at 400–500 °C, sulfur dissolution decreased, which indicated the formation of sulfate phases insoluble in the acid leach medium, consistent with the information described next in Table 7.

3.2.2. *Characterisation of baked solids and leach residues by XRD*

Iron and rare earth phases identified by XRD analysis of the baked mixtures and leach residues are summarised in Table 7. The species are listed in approximate order of abundance within each solid sample. At low bake temperatures, hydrated acidic ferric sulfates, anhydrous ferric sulfates and hydrated rare earth sulfate, of molecular formulae: $HFe(SO_4)_2 \bullet 4H_2O$, $Fe_2(SO_4)_3$, $Ce_2(SO_4)_3 \bullet 8H_2O$, were formed. In certain samples, rare earth sulfates were not detected, indicating they were amorphous. After baking at 400–500 °C, all hydrated ferric and rare earth sulfates were dehydrated to their anhydrous forms. Anhydrous rare earth sulfate remained in the bake solid up to 800 °C. After baking at 800 °C, the rare earth sulfate appeared to be partially decomposed, with the XRD reflections decreasing slightly in intensity, while new reflections due to monazite ($CePO_4$) and/or CeO_2 appeared, depending on the iron mineral. After baking at 800 °C, anhydrous ferric sulfate had decomposed and Fe_2O_3 and/or $FePO_4$ were detected.

An example of a XRD pattern of acid-baked solids of monazite with goethite (1:1 *w*/w) at 800 °C is provided in Fig. 5. The re-formed monazite ($CePO_4$) present in the leach residues (Table 7 and Fig. 5) explains the decrease in rare earth and phosphorus dissolution after baking at 800 °C. Iron(III) phosphate was not detected in the XRD patterns of leach residues, indicating that it was soluble in the 0.9 M sulfuric acid leach, hence the dissolution of a portion of the iron even after baking at 800 °C (Fig. 3). In

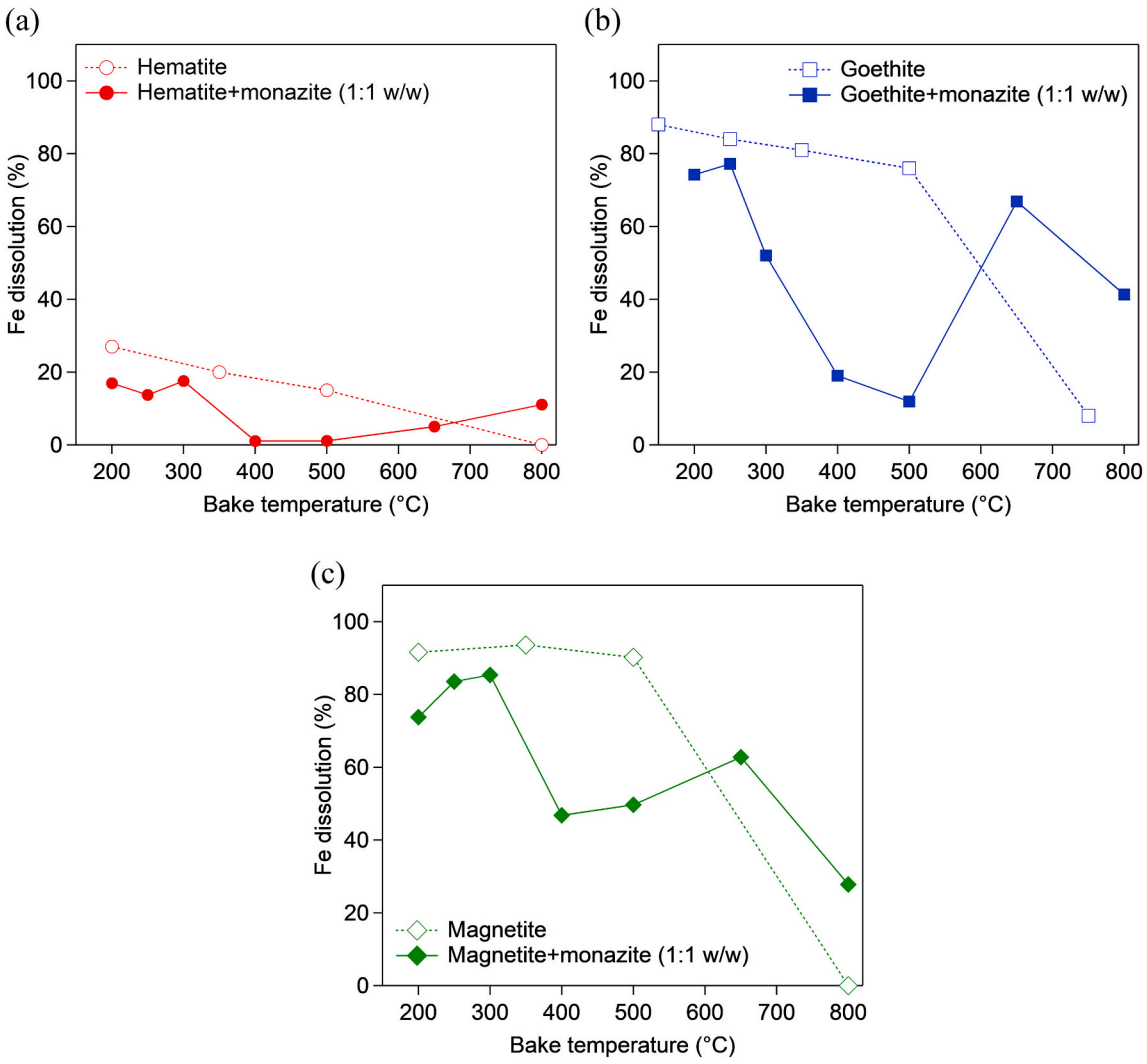

Fig. 3. Iron dissolution for acid baking and leaching of iron minerals individually compared with a 1:1 (*w*/w) mixture with monazite for (a) hematite, (b) goethite and (c) magnetite

the goethite-monazite bakes, insoluble rare earth and thorium oxides (CeO_2, $Th_{0.5}Ce_{0.5}O_2$) were formed at 800 °C, further contributing to low rare earth and thorium dissolution (Fig. 2).

Anhydrous ferric sulfate of monoclinic or rhombohedral crystal structures were detected in leach residues from bakes at 400–650 °C. The presence of these salts, denoted by T-$Fe_2(SO_4)_3$ or M-$Fe_2(SO_4)_3$ in Table 7 and Fig. 6, partially explain the decrease in iron and sulfur dissolution after baking at 400–650 °C in Fig. 3-4. The XRD patterns of the bake solids and leach residues from acid bakes of goethite with monazite at 300 °C and 500 °C are given in Fig. 6. The ferric sulfates formed at 300 °C were practically absent in the XRD pattern of the leach residue, while those formed at 500 °C were a major phase in the corresponding leach residue. The failure of the ferric sulfates to completely dissolve in the leach medium after baking at 500 °C was not observed during acid baking of the iron minerals individually (Fig. 3) and was therefore related to the presence of monazite. Leaching may be inhibited if the iron sulfates are finely intergrown with insoluble reaction products formed in the iron mineral/monazite bake.

No phosphate species were identified by XRD in baked solids or leach residues until the bake temperature reached 800 °C as evident from Table 7. It was therefore unclear from the XRD data what types of reaction products were responsible for the decrease in leaching of phosphorus after baking at temperatures of 400–500 °C.

3.2.3. *Characterisation of baked solids and leach residues by SEM-EDS*

(a) *Formation of iron sulfate-polyphosphate type phase at 400–500 °C*

Phosphorus dissolution in the leach medium decreased abruptly after baking at 400–500 °C (Fig. 4b). The SEM-EDS analysis showed that phosphorus was mainly present within an ill-defined, amorphous phase containing iron, phosphorus, and varying amounts of sulfur in addition to some thorium after baking at 400–500 °C (Fig. 7). Rare earth elements were detected as a minor component of this phase (Fig. 7b), causing the ~10% decrease in rare earth dissolution after baking at 400–500 °C compared to 300 °C (Fig. 2). The ratio of phosphorus to oxygen in this phase was estimated based on its average elemental composition determined by EDS. Oxygen content was calculated indirectly using the method of assumed stoichiometry of cations (charge balance of cations to anions) as mentioned by Newbury et al. (1995) and quoted by Newbury and Ritchie (2013). It was assumed that sulfur was present as sulfate. By this method, the elemental composition was indicative of a polyphosphate type species, e.g. $Fe(PO_3)_3$ (Table 8). The phase was therefore designated as an "iron sulfate-polyphosphate" type phase in Fig. 7. Due to the limitations of standardless EDS, only qualitative identification of phases is possible and hence the designation is indicative only.

The overall significant improvement in rare earth extraction from

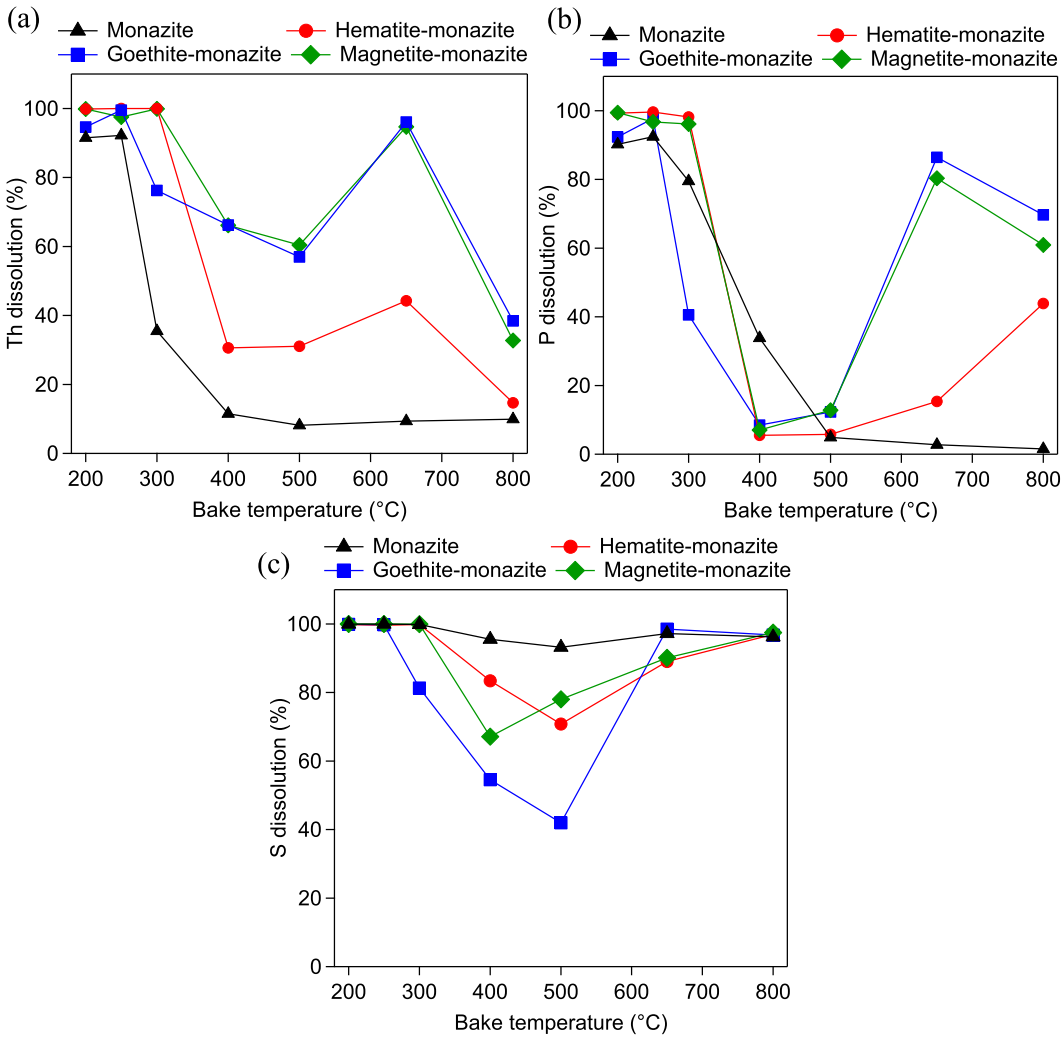

Fig. 4. Effect of bake temperature on (a) Th, (b) P and (c) S dissolution for mixtures of monazite with goethite, hematite and magnetite (1:1 w/w), compared with monazite alone (Bake conditions: 250% stoichiometric acid addition for monazite, 200% stoichiometric acid addition for monazite-iron mineral mixtures where stoichiometric addition is defined as the acid required to react with all cations; Leach conditions: 0.9 M H_2SO_4, liquid to solid ratio of 40:1 w/w), 2 h, 20–25 °C).

iron mineral/monazite baked mixtures relative to acid baking of monazite alone can be attributed to the formation of this amorphous iron sulfate-polyphosphate type phase in preference to the amorphous thorium and rare earth containing polyphosphate phase formed during sulfuric acid baking of monazite alone (Demol et al., 2018), which had a much higher rare earth content. In effect, iron compounds react with phosphate compounds in the bake, thereby allowing the rare earth elements and part of the thorium to remain as soluble sulfates.

After leaching, the iron and sulfur contents in the iron sulfate-polyphosphate phase noticeably increased e.g. from an atomic ratio of S/P of 0.29 in the bake solid to 0.63 in the leach residue (Table 8). This occurred for each of the iron mineral/monazite mixtures. Using the method of assumed stoichiometry of cations to calculate the oxygen to phosphorus ratio, the phase composition was closer to pyrophosphate ($Fe_4(P_2O_7)_3$) with sulfate. Under the SEM, the appearance of the phase was similar before and after leaching, and the phase did not appear to be a precipitate. Li et al. (2009) claimed in a patent that iron pyrophosphate is formed in a 300 °C acid bake of monazite ore, although no data was given. Further work is required to identify this phase more accurately.

In the present work, hematite had a smaller effect on rare earth dissolution after baking at temperatures above 300 °C compared to goethite and magnetite (Fig. 2) which may be due to the lower extent of hematite sulfation compared to goethite and magnetite. This is likely to lead to a lower availability of 'sulfated iron' to form an iron sulfate-polyphosphate type phase during acid bakes of monazite with hematite. The amorphous iron sulfate-polyphosphate type phase formed from the magnetite/monazite and goethite/monazite combinations contained more sulfur than that of the hematite/monazite combination, as indicated by the descending order of the sulfur content of this phase in Table 9 (goethite>magnetite>hematite at 400 and 650 °C). Due to the limited resolution of EDS measurement (~3 μm) it was not clear whether this sulfate was part of the polyphosphate or due to a very closely intergrown ferric sulfate phase. Fig. 8 shows two phases of differing composition, which are ferric sulfate intergrown with the iron sulfate-polyphosphate type phase, for monazite/magnetite solids from the 400 °C bake. It is possible that the sulfur in the iron polyphosphate phase may be very fine ferric sulfate that is below the resolution of EDS measurement. Alternatively, the sulfur may be present as SO_4^{2-} ions incorporated within the amorphous iron polyphosphate structure, which would make it a sulfophosphate compound of the type described in Bingham and Hand (2008). This could not be confirmed in the current study.

(b) *Alteration of iron sulfate-polyphosphate type phase at 650 °C*

After baking at 650 °C, there was a change in composition of the iron sulfate-polyphosphate type phase as it was more soluble in the leach medium. Thus, it was only a minor remnant component of the leach

Table 7
Dissolution of Fe, P, Th and total rare earth elements and phases identified in bake products and leach residues of iron mineral/monazite mixtures by XRD analysis.

Iron mineral[a]	Temp. (°C)	Species identified by XRD		Dissolution (%)			
		Bake solids	Leach residue	Fe	P	Th	TRE
Hematite	200	Fe_2O_3	Fe_2O_3	17	99	100	100
	250	$Ce_2(SO_4)_3.8H_2O$, Fe_2O_3	Fe_2O_3	14	100	100	100
	300	$HFe(SO_4)_2.4H_2O$, $Ce_2(SO_4)_3.8H_2O$, Fe_2O_3,	Fe_2O_3	18	98	100	100
	400	T-$Fe_2(SO_4)_3$, M-$Fe_2(SO_4)_3$, Fe_2O_3,	Fe_2O_3	1	5	31	89
	500	$Ce_2(SO_4)_3$, T-$Fe_2(SO_4)_3$, M-$Fe_2(SO_4)_3$, Fe_2O_3,	Fe_2O_3, M-$Fe_2(SO_4)_3$	1	6	31	88
	650	$Ce_2(SO_4)_3$, T-$Fe_2(SO_4)_3$, M-$Fe_2(SO_4)_3$, Fe_2O_3,	Fe_2O_3, M-$Fe_2(SO_4)_3$	5	15	44	82
	800	$Ce_2(SO_4)_3$, $La_2(SO_4)_3$, $FePO_4$, $CePO_4$, Fe_2O_3,	$CePO_4$, Fe_2O_3,	11	44	15	64
Goethite	200	M-$Fe_2(SO_4)_3$	FeO(OH)	74	92	95	94
	250	M-$Fe_2(SO_4)_3$	FeO(OH)	77	98	100	99
	300	M-$Fe_2(SO_4)_3$, T- $Fe_2(SO_4)_3$	M- $Fe_2(SO_4)_3$	52	41	76	97
	400	$Ce_2(SO_4)_3$, M-$Fe_2(SO_4)_3$, T-$Fe_2(SO_4)_3$	M-$Fe_2(SO_4)_3$, T-$Fe_2(SO_4)_3$,	19	8	66	93
	500	$Ce_2(SO_4)_3$, M-$Fe_2(SO_4)_3$, T-$Fe_2(SO_4)_3$	M-$Fe_2(SO_4)_3$, T-$Fe_2(SO_4)_3$,	12	12	57	92
	650	$Ce_2(SO_4)_3$, M-$Fe_2(SO_4)_3$, T-$Fe_2(SO_4)_3$	Fe_2O_3	67	86	96	96
	800	$Ce_2(SO_4)_3$, $FePO_4$, $CePO_4$, Fe_2O_3, CeO_2	Fe_2O_3, $CePO_4$, CeO_2, $Th_{0.5}Ce_{0.5}O_2$	41	70	38	68
Magnetite	200	$HFe(SO_4)_2.4H_2O$	Fe_2O_3, Fe_3O_4	74	99	100	100
	250	$HFe(SO_4)_2.4H_2O$	Fe_2O_3, Fe_3O_4	84	97	98	97
	300	$Ce_2(SO_4)_3.7.5H_2O$		85	96	100	100
	400	M-$Fe_2(SO_4)_3$,	M-$Fe_2(SO_4)_3$	47	7	66	92
	500	M-$Fe_2(SO_4)_3$, $Ce_2(SO_4)_3$	M-$Fe_2(SO_4)_3$	50	13	60	90
	650	M-$Fe_2(SO_4)_3$, $Ce_2(SO_4)_3$	M-$Fe_2(SO_4)_3$, $CePO_4$	63	80	95	91
	800	Fe_2O_3, $Ce_2(SO_4)_3$, $CePO_4$	Fe_2O_3, $CePO_4$	28	61	33	63

M- $Fe_2(SO_4)_3$: Monoclinic ferric sulfate; T- $Fe_2(SO_4)_3$: Trigonal-rhombohedral ferric sulfate.
[a] Baked as a 1:1 w/w mixture of monazite : iron mineral and H_2SO_4 as described in Table 1

residues. Fig. 9 compares the EDS spectra of this phase from the magnetite/monazite (1:1 w/w) bakes at 400 °C and 650 °C. Average elemental compositions based on EDS of the iron sulfate-polyphosphate type phases formed at 400 °C and 650 °C are presented in Table 9. The main differences between the phases were an increase in iron content and a decrease in phosphorus and sulfur content after baking at the higher temperature of 650 °C, compared to 400 °C, as shown for hematite and magnetite in Table 9.

Assuming that sulfur is present as sulfate in the iron sulfate-polyphosphate type phase, calculation of oxygen content relative to phosphorous using the method of assumed stoichiometry indicated an increase in oxygen to phosphorus ratio. However, the phase composition was variable and was also dependent on the iron mineral. This change in phosphate speciation at 650 °C was accompanied by a dramatic increase in phosphorus dissolution, particularly for the goethite and magnetite mixtures with monazite (Fig. 4b). This implied the new iron sulfate-polyphosphate type phase was much more soluble during leaching.

The decrease in sulfate content associated with the polyphosphate phase was consistent with the ferric sulfate decomposition temperature of 500–700 °C (Mu and Perlmutter, 1981; Tagawa, 1984). A mechanism is proposed where the sulfate associated with the amorphous iron polyphosphate phase begins to partially react and release sulfur trioxide gas, leading to the formation of iron orthophosphate instead of the usual decomposition product iron oxide as shown in Eq. (2). The polyphosphate species in Eq. (2), ($Fe(PO_3)_3$), does not represent the actual polyphosphate formed in this study, which was amorphous and could not be fully characterised using the techniques available. The net overall reaction, from ferric sulfate to ferric phosphate, is shown in Eq. (3):

$$Fe_2(SO_4)_3{\cdot}Fe(PO_3)_3 \rightarrow 3FePO_4 + 3SO_3(g) \quad (2)$$

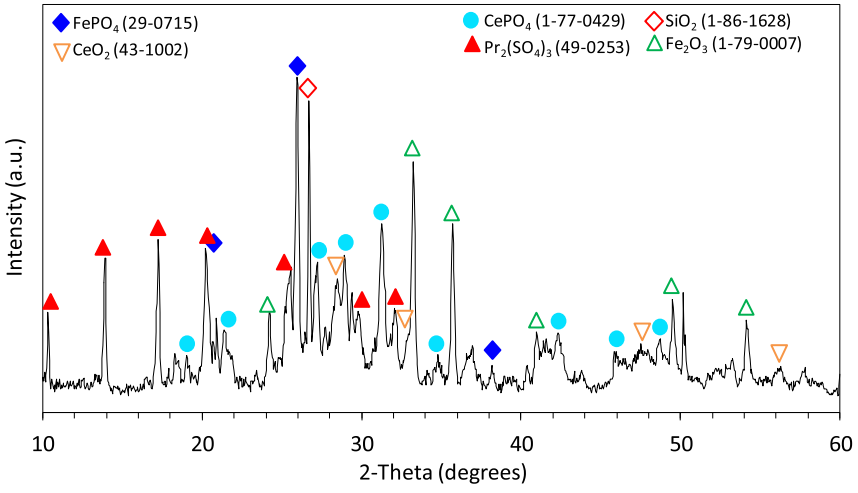

Fig. 5. XRD pattern of acid baked solids of 1:1 (*w*/w) mixture of monazite with goethite at 800 °C (also see Table 7).

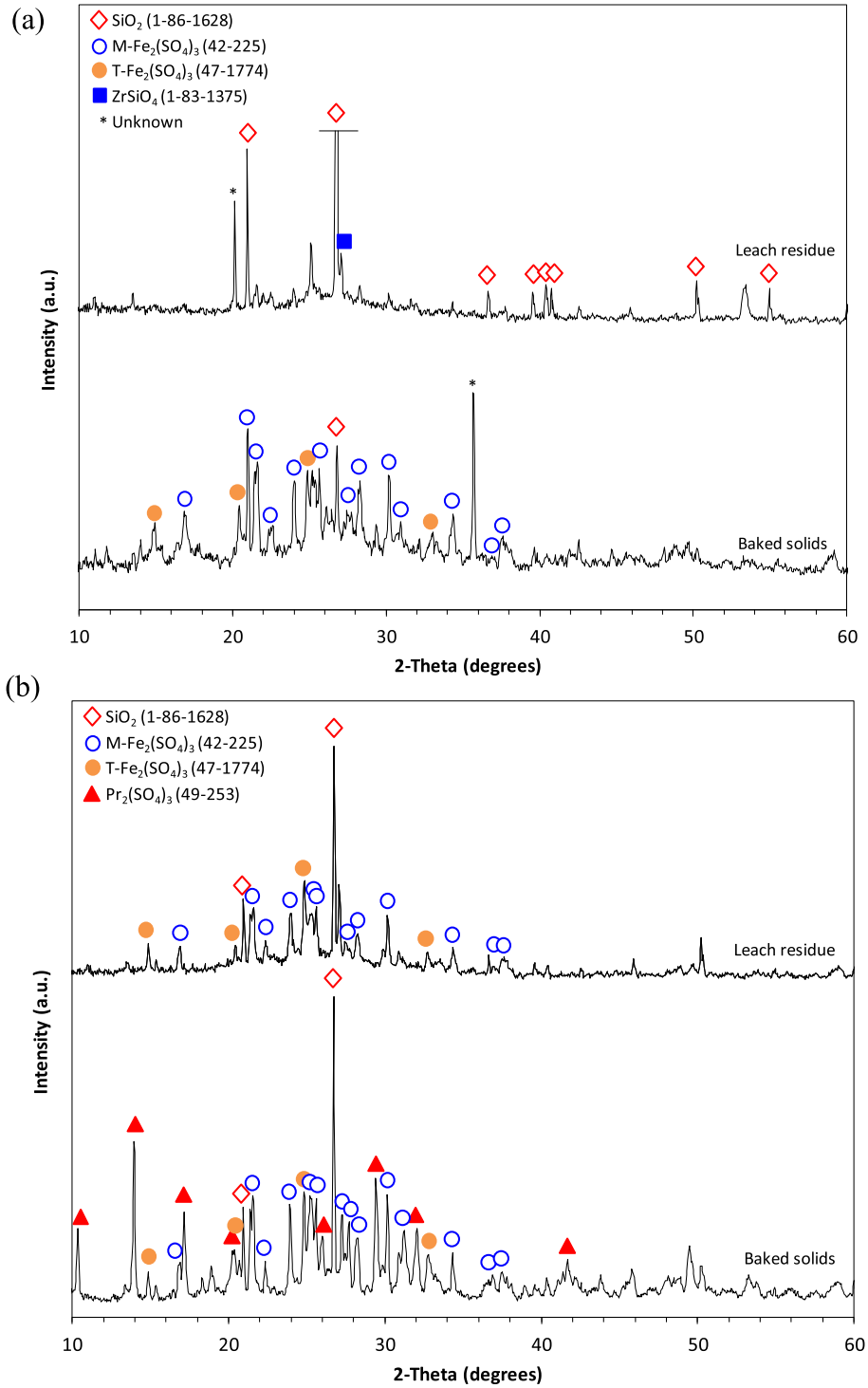

Fig. 6. XRD patterns of acid bake solids of goethite with monazite (1:1 *w*/w) at 300 °C and 500 °C showing the presence of $Fe_2(SO_4)_3$ in both baked solids and (a) showing deficiency of $Fe_2(SO_4)_3$ in leach residue produced from 300 °C bake and (b) showing presence of ferric sulfates in leach residue produced from 500 °C bake.

$$Fe_2(SO_4)_3 + H_3PO_4 \rightarrow 3FePO_4 + 3SO_3(g) + 3H_2O(g) \quad (3)$$

The standard Gibbs free energy (ΔG^o) of reaction for Eq. (3) in the temperature range of 0–1000 °C is shown in Fig. 10. The data show that the reaction becomes thermodynamically favourable for temperatures greater than approximately 520 °C.

(c) *Formation of thorium/cerium oxide at 800 °C*

The SEM-EDS analysis of the solids produced after baking at 800 °C showed that light coloured particles (with higher BSE intensity) had formed as inclusions within the rare earth sulfate phase (Fig. 11). The resolution of the EDS was insufficient to provide a pure spectrum of the inclusions. However, from the significant enrichment of thorium in the EDS spectrum, it was concluded that the embedded particles may contain thorium oxide (ThO_2) or a thorium phosphate (Fig. 11b). Further evidence comes from a solid phase with composition $Th_{0.5}Ce_{0.5}O_2$ detected by XRD in the 800 °C bake solids and leach

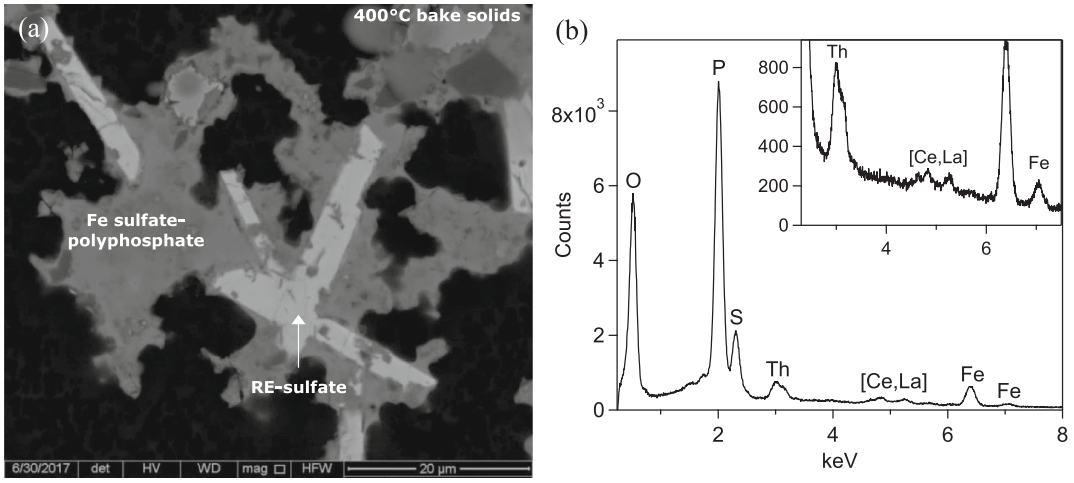

Fig. 7. Back scattered electron (BSE) image and EDS spectrum of iron sulfate-polyphosphate type phase formed during acid baking of monazite with hematite (1:1 *w*/w) at 400 °C.

Table 8
Average composition by EDS of iron sulfate-polyphosphate phase before and after leaching.

Solid sample[a]	Atomic ratios[b] (normalised to P)						
	Al	Ce,La	Fe	P	Si	S	Th
Bake solids	0.01 ± 0.004	0.05 ± 0.01	0.31 ± 0.01	1.00 ± 0.09	0.07 ± 0.03	0.29 ± 0.03	0.03 ± 0.002
Leach residue	0.01 ± 0.01	0.02 ± 0.01	0.84 ± 0.02	1.00 ± 0.03	0.08 ± 0.03	0.63 ± 0.07	0.08 ± 0.03

[a] From 400 °C bake of hematite with monazite (1:1 *w*/w).
[b] Average of 5 EDS measurements. Ranges represent ± one standard deviation.

Table 9
Average elemental composition by EDS of iron sulfate-polyphosphate type phases in acid-baked solids of iron mineral/monazite mixtures.

Iron mineral[a]	Bake temp. (°C)	Atomic ratios in bake products (moles, normalised to P)[b]						
		Al	Ce,La	Fe	P	Si	S	Th
Hematite	400	0.01 ± 0.004	0.05 ± 0.01	0.31 ± 0.01	1.00 ± 0.09	0.07 ± 0.03	0.29 ± 0.03	0.03 ± 0.002
	650	0.02 ± 0.01	0.07 ± 0.01	0.47 ± 0.03	1.00 ± 0.09	0.07 ± 0.02	0.12 ± 0.07	0.02 ± 0.006
Goethite	650	0.07 ± 0.02	0.13 ± 0.04	1.97 ± 0.06	1.0 ± 0.25	0.2 ± 0.12	1.1 ± 0.3	–
Magnetite	400	0.004 ± 0.003	0.05 ± 0.02	0.6 ± 0.15	1.0 ± 0.17	0.06 ± 0.01	0.7 ± 0.1	0.006 ± 0.004
	650	0.02 ± 0.01	0.05 ± 0.01	1.1 ± 0.12	1.0 ± 0.16	0.08 ± 0.04	0.42 ± 0.07	0.010 ± 0.008

[a] Baked at 1:1 w/w ratio of monazite and iron mineral.
[b] Average of 5 EDS measurements; uncertainties represent ± one standard deviation.

residue produced from the goethite/monazite bake (Table 7).

Calculated thermodynamic equilibrium compositions for cerium, lanthanum and thorium sulfate species distribution between 500 °C and 1200 °C based on HSC Chemistry version 8 are given in Fig. 12. The initial relative concentrations were based on the concentrations of Ce, La and Th in the bake feed mixture. Decomposition of $Ce_2(SO_4)_3$ to CeO_2 becomes thermodynamically favourable at temperatures ≥800 °C. It is predicted that $La_2(SO_4)_3$ decomposes to La_2O_3 at a much higher temperature, ≥1070 °C. The decomposition of $Th(SO_4)_2$ to ThO_2 is predicted to occur at temperatures ≥900 °C, and would therefore not be expected during the 800 °C bake. These results suggest that the thorium-rich phase observed in the 800 °C goethite/monazite (1:1 *w*/w) bake solids may be a combination of CeO_2 and thorium phosphate. It is also possible that the thorium was incorporated within the CeO_2 structure as suggested by the identification of the solid phase $Ce_{0.5}Th_{0.5}O_2$ by XRD noted in Table 7.

3.3. Characterisation of leach residues by infrared spectroscopy

The leach residues produced after acid bakes of monazite with magnetite at 300 to 800 °C were analysed by FT-IR to further investigate the speciation of the insoluble phases observed by SEM-EDS. An overlay of the spectra is presented in Fig. 13. The peaks at 950 and 995 cm^{-1}, appearing in the 800 °C bake solid, are characteristic of orthophosphate vibrations in monazite (Demol et al., 2018), providing additional evidence for the re-forming of a monazite phase during baking at the temperature of 800 °C. The strong band appearing at 700–650 cm^{-1} is due to iron oxide (Socrates, 2001), formed from the decomposition of iron sulfate in the 800 °C bake.

The spectra of the leach residues produced from the 400–500 °C bakes of monazite with magnetite were not as well defined, due to the overlap of a number of bands. Deconvolution was carried out for the leach residue produced from the 500 °C bake in an attempt to better define the bands involved (Fig. 14), with the assignments listed in Table 10. Vibrations corresponding to orthophosphate, polyphosphate, sulfate and hydroxyl groups were assigned. The presence of polyphosphate (P-O-P) bands supported the presence of an iron polyphosphate after baking at 400–500 °C, as proposed, based on the SEM-EDS results. The presence of sulfate vibrations was consistent with the presence of insoluble $Fe_2(SO_4)_3$ in the leach residue, as indicated by XRD data in Table 7. The presence of hydroxyl (M-OH) groups and coordinated water is indicative of alterations to phases during leaching, as

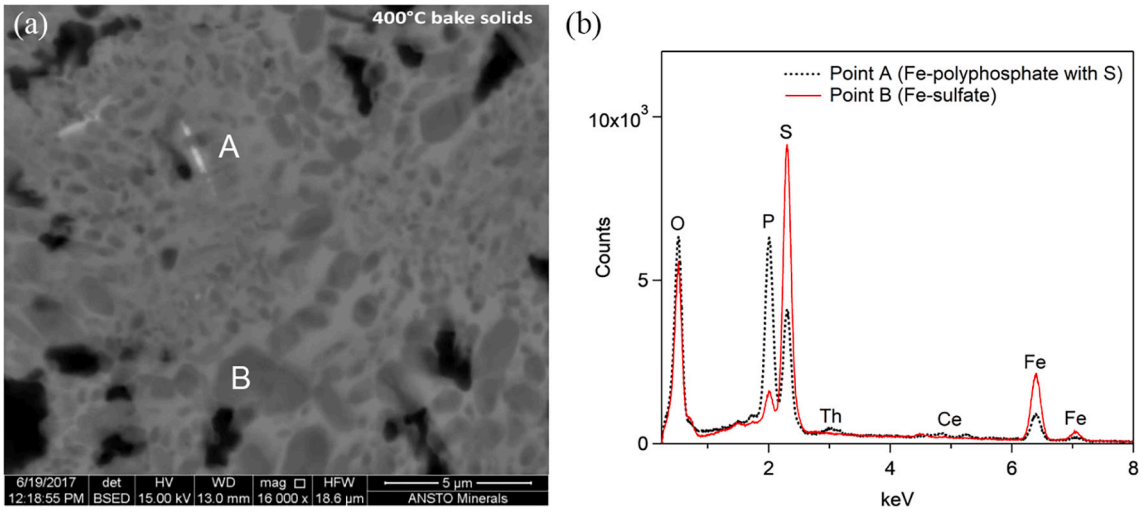

Fig. 8. BSE image and EDS spectra of sulfate-containing iron polyphosphate phase with impregnated iron sulfate, formed during acid baking of monazite with magnetite (1:1 *w*/w) at 400 °C.

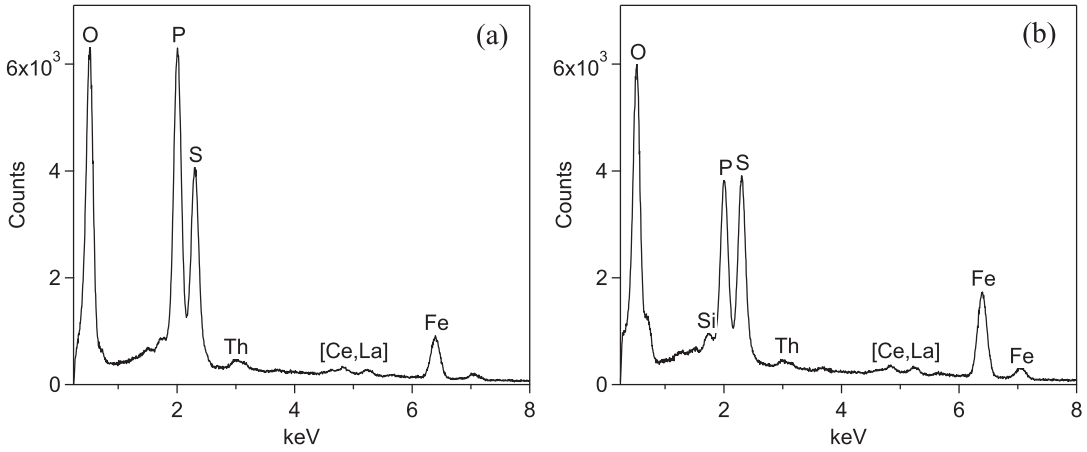

Fig. 9. EDS spectra of sulfate-containing iron polyphosphate phase from acid baking of magnetite with monazite (1:1 w/w) at (a) 400 °C and (b) 650 °C.

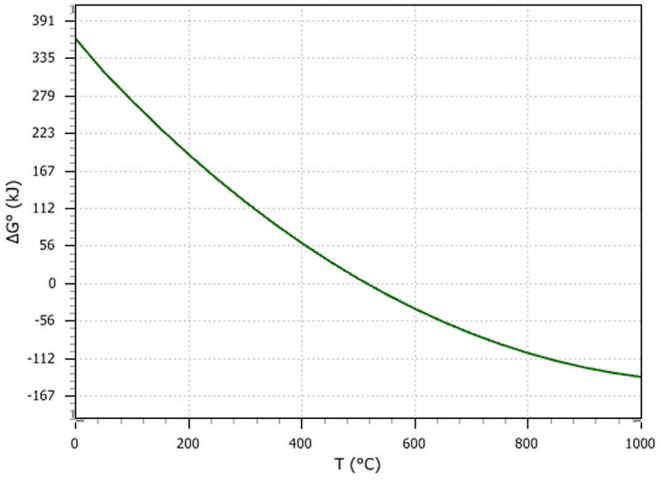

Fig. 10. Gibbs free energy (ΔG^o) of overall reaction for the conversion of iron sulfate ($Fe_2(SO_4)_3$) to iron phosphate ($FePO_4$) (Data from HSC Chemistry, version 8.0).

these groups are unlikely to be stable in the bake solid during treatment at 500 °C. These phases must be amorphous, as there were no hydroxylated species identified by XRD in this leach residue (Table 7).

3.4. Thermogravimetric analyses of iron mineral/monazite/acid mixture

The thermogravimetric analyses of sulfuric acid with 1:1 (*w*/w) mixtures of monazite with each iron mineral are given in Fig. 15a-c. The curves were similar for each of the iron mineral monazite combinations. Thermogravimetric analyses of individual iron minerals are shown in Appendix B. Six endothermic processes were observed, each with an associated loss of mass due to the generation of gaseous reaction products. Proposed reactions corresponding to each thermal event, based on characterisation of the reaction products as presented herein, are summarised in Table 11.

The endothermic event at 147–177 °C was assigned to the reactions of the iron mineral and monazite with sulfuric acid, forming the sulfates of iron, rare earth and thorium as identified by XRD (Section 3.2.2). These reactions (Eqs. 4,5,6,7,8) have been previously reported (Wang et al., 2010). The mass loss can be attributed to volatilisation of the water formed in Eqs. 4–6 and the initiation of slow dehydration of the orthophosphoric acid formed in Eqs. 7–8.

The endotherm and mass loss at 257–261 °C is attributed to the volatilisation of sulfuric acid, as demonstrated in previous work (Demol

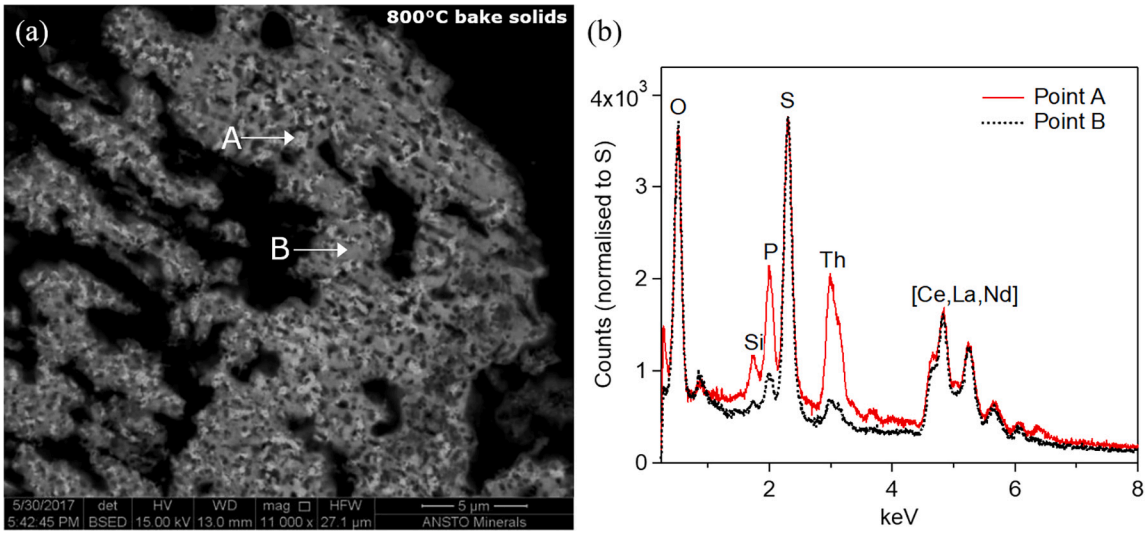

Fig. 11. BSE image and EDS spectra of rare earth-sulfate and Th,Ce-oxide phases after acid baking monazite with goethite at 800 °C.

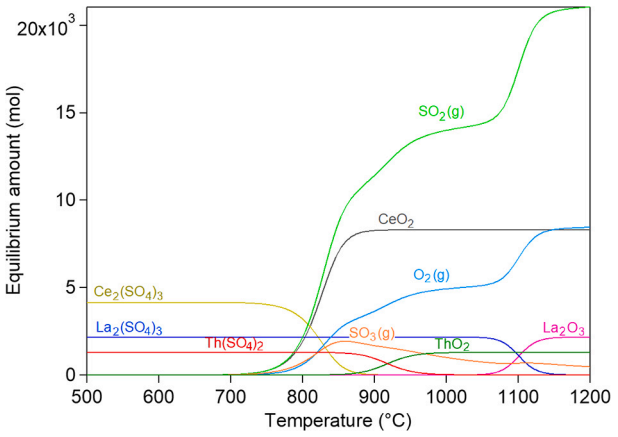

Fig. 12. Effect of temperature on species distribution due to thermal decomposition of rare earth and thorium sulfates (calculated using HSC Chemistry version 8, assuming inert atmosphere, initial concentrations of 1.29 kmol $Th(SO_4)_2$, 2.16 kmol $La_2(SO_4)_3$ and 4.15 kmol $Ce_2(SO_4)_3$).

et al., 2018). The high air purge used in the thermogravimetric analysis likely contributed to the lower temperature of acid volatilisation, which is below the boiling point of sulfuric acid, since it would sweep away any acid vapour or gases above liquid sulfuric acid. Schwartz et al. (2000) and Soltani et al. (2018) predict some H_2SO_4 gas in equilibrium above liquid H_2SO_4 at these temperatures. The dehydration of orthophosphoric acid via Eqs. (11−13) would also be occurring in this temperature range (Demol et al., 2018).

The thermal event at 322–326 °C was attributed to formation of the iron sulfate-polyphosphate type phase identified by SEM-EDS of the baked solids produced in the temperature range 400–500 °C (Section 3.2.3). This compound is represented as $Fe_2(SO_4)_3 \bullet 2Fe(PO_3)_3$, but its exact formula could not be determined by the available analytical techniques. In the 350 °C to 600 °C temperature region, there was a distended event with a slight mass loss. This event could not be conclusively identified. It is possible that there was a slow release of sulfur trioxide from the iron sulfate-polyphosphate type phase. The reactions for the 659–679 °C event are not confirmed but decomposition of ferric sulfate occurs at these temperatures (Mu and Perlmutter, 1981; Tagawa, 1984; Siriwardane et al., 1999), and is a likely contributor. The SEM-EDS analyses also indicated that an alteration of the iron sulfate-polyphosphate to a possible iron orthophosphate occurred during the

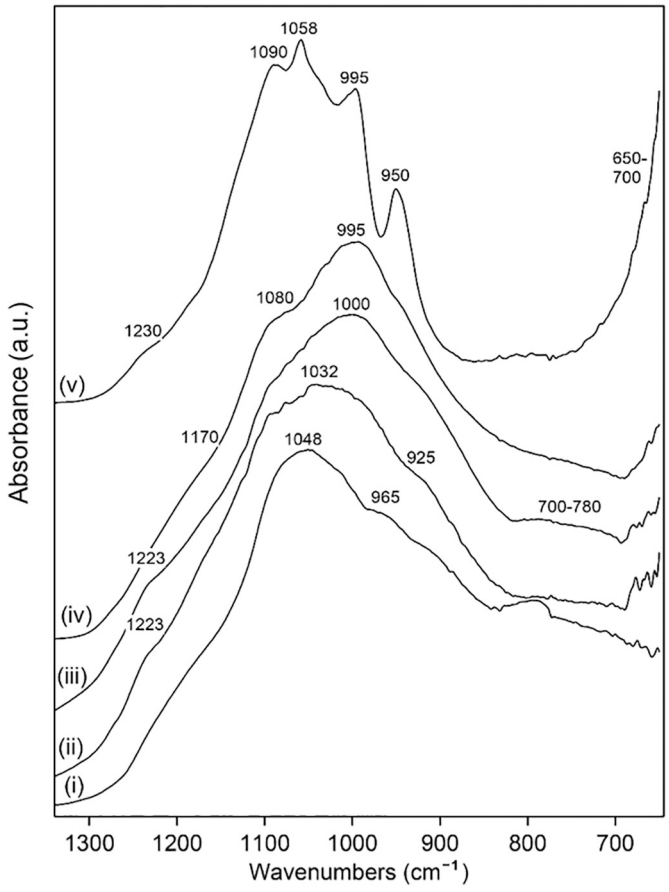

Fig. 13. FT-IR spectra of leach residues after baking monazite with magnetite at (i) 300 °C, (ii) 400 °C, (iii) 500 °C, (iv) 650 °C and (v) 800 °C and acid leaching.

650 °C bake, which may also have contributed to the 659–679 °C thermal event. The reaction in Eq. (2) is proposed. The final thermal event appeared to actually consist of a series of overlapping events between 700 °C and 900 °C. This event was attributed to formation of monazite and cerium(IV)-thorium(IV) oxide via Eqs. 16–17, based on the identification of these phases by XRD (Table 7).

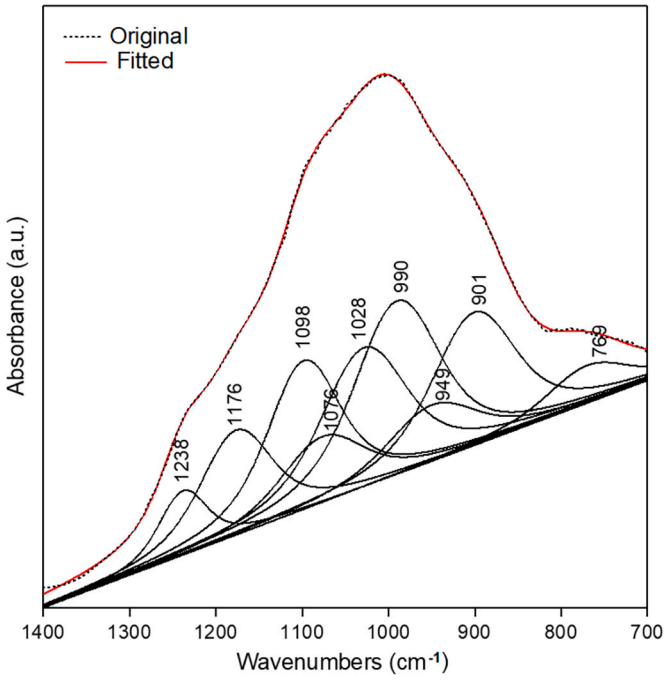

Fig. 14. Deconvolution of FT-IR spectrum of leach residue produced from 500 °C bake of monazite with magnetite.

Table 10
Assignments for deconvoluted FT-IR spectrum of leach residue produced from 500 °C bake of monazite with magnetite.

IR peak (cm^{-1})	Peak assignment	Comments	Reference
1238	δ(OH), in M-OH	Deformation (bending) of hydroxyl groups	[a]
1176, 1098, 1076, 1028	$\nu_{as}(SO_4^{2-})$ + $\nu_{as}(PO_4^{3-})$, ν(P-O-P)	Asymmetric stretching vibrations	[a,b]
990, 949	$\nu_s(SO_4^{2-})$ + $\nu_s(PO_4^{3-})$, ν(P-O-P)	Symmetric stretching vibrations	[a,b,c,d]
901	ν(P-O-P)	Stretching vibration	[e]
769	δ(HOH)	Vibration modes of coordinated water molecules	[a]

[a] Socrates (2001).
[b] Frost et al. (2014).
[c] Da et al. (2011).
[d] Möncke et al. (2014).
[e] Dacheux et al. (2005).

3.5. Implications for rare earth processing

The data presented in this work provides useful insights and supporting evidence of high temperature reactions that are occurring in acid baking of monazite where iron minerals are present, and how this knowledge might be applied in commercial practice. The goal of any successful rare earth process is to maximise recovery of rare earth elements and rejection of impurities. If impurities, including radioactive thorium, can be separated from the rare earths in the bake step this would generally translate to simplified downstream purification processing. The first generation acid bake plants in China used low temperature rare earth sulfation (200–300 °C), with high recovery of rare earths to the leach liquor along with thorium, iron and phosphorus. The separation of these impurities has complicated and compromised rare earth recovery in downstream processing (Zhang et al., 2015). In second and third generation acid bake processes, higher temperatures (up to 800 °C) were introduced to control rejection of these impurities to the leach residue (Zhang et al., 2015). However, the specific role of iron in

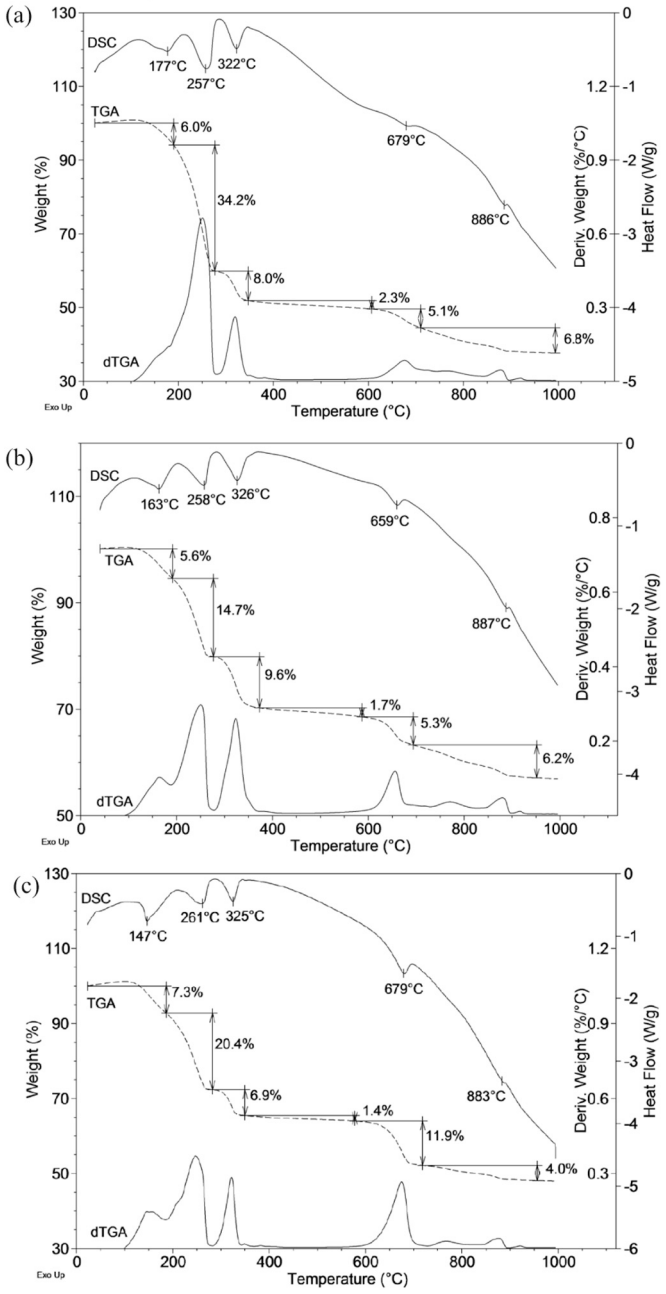

Fig. 15. Thermogravimetric analysis (TGA) and Differential Scanning Calorimetry (DSC) of 1:1 (w/w) mixtures of monazite and (a) hematite, (b) goethite and (c) magnetite with sulfuric acid (150% stoichiometric acid addition, 5–10 °C/min, 20 mL/min air purge).

these processes has not always been clear. The patent literature has made specific reference to the benefits of an increased iron content in monazite rich concentrates (e.g. 8–40 wt% Fe) such as those found in Mt. Weld, Australia. The benefits include an improved rare earth recovery at temperatures of 230–600 °C, and purification of liquors with simple neutralisation (Li et al., 2009). In another example, targeting sulfation of gangue minerals containing iron or aluminium at low temperature followed by conversion to insoluble phosphates at higher temperature co-occurring with sulfation of monazite (650–750 °C), was claimed to reduce acid consumption compared to the high temperature Chinese process (Teixeira and Silva, 2015). The addition of Fe(III) to react with phosphate present in the water leach liquor prior to neutralisation to prevent co-precipitation of rare earths has also been proposed in process

Table 11
Proposed reactions for thermal events observed by TG-DSC analysis of monazite/iron mineral mixtures with sulfuric acid.

Temp. (°C)	Proposed processes/reactions	ΔG^{o}_{rxn} (kJ)[a]	Eq. no.
147–177	$2FeO(OH) + 3H_2SO_4 \rightarrow Fe_2(SO_4)_3 + 4H_2O(g)$	−187	4
	$Fe_2O_3 + 3H_2SO_4 \rightarrow Fe_2(SO_4)_3 + 3H_2O(g)$	−176	5
	$2Fe_3O_4 + 10H_2SO_4 \rightarrow 3Fe_2(SO_4)_3 + SO_2(g) + 10H_2O(g)$	−601	6
	$2LaPO_4 + 3H_2SO_4 \rightarrow La_2(SO_4)_3 + 2H_3PO_4$	−53	7
	$Th_3(PO_4)_4 + 6H_2SO_4 \rightarrow 3Th(SO_4)_2 + 4H_3PO_4$	−573	8
257–261	$H_2SO_4(l) \rightarrow H_2SO_4(g)$	7	9
	$H_2SO_4(l) \rightarrow SO_3(g) + H_2O(g)$	27	10
	$nH_3PO_4 \rightarrow H_{n+2}P_nO_{3n+1} + nH_2O(g)$	–	11
	$nH_3PO_4 \rightarrow (HPO_3)_n + nH_2O(g)$	–	12
	$H_3PO_4 \rightarrow HPO_3 + H_2O(g)$	–	13
322–326	$6HPO_3 + 3Fe_2(SO_4)_3 \rightarrow 2Fe_2(SO_4)_3\text{-}2Fe(PO_3)_3 + SO_3(g) + 3H_2O(g)$	–	14
350–600	Unknown[b]		15
659-679	$Fe_2(SO_4)_3{\cdot}Fe(PO_3)_3 \rightarrow 3FePO_4 + 3SO_3(g)$	–	2
700–900	$2Fe_2(SO_4)_3{\bullet}2Fe(PO_3)_3 + Ln_2(SO_4)_3 \rightarrow 2LnPO_4 + 4FePO_4 + Fe_2O_3 + 6SO_3(g)$	–	16
	$Ce_2(SO_4)_3 + 2Th(SO_4)_2 + ½O_2 \rightarrow 4Ce_{0.5}Th_{0.5}O_2 + 7SO_3(g)$	–	17

[a] Gibbs free energy change was calculated for reactions where thermodynamic data was available. The temperature used in calculation corresponding to the thermal event in Fig. 15 (160 °C for 147–177 °C, 260 °C for 257–261 °C, 670 °C for 659–679 °C and 800 °C for 700–900 °C).
[b] Possibly slow removal of sulfate from amorphous iron sulfophosphates as $SO_3(g)$.

options for both the Nolans and Browns Range projects in Australia. One patent makes specific mention of the possibility of ferric addition to the bake as a means of improving rare earth recovery but provides no specific examples (Mackowski et al., 2009). The current work provides a theoretical and evidence based explanation as to why the presence of particular iron minerals in the concentrate is beneficial for phosphate sequestration. This in turn is helpful in achieving the dual objective of high rare earth recovery and impurity rejection in the acid bake/water leach process.

4. Conclusions

The main finding of this work was that there was a significant improvement in rare earth extraction from bake reaction products of the iron mineral/monazite mixtures after baking at 400–500 °C, compared to acid baking of monazite alone. The beneficial effect can be attributed to the formation of an amorphous iron sulfate-polyphosphate type phase in preference to the thorium and rare earth containing polyphosphates formed during acid baking of monazite. The addition of iron minerals to an iron-free monazite concentrate caused an improvement in rare earth solubility in the leach medium, whilst achieving significant rejection of phosphorus and to some extent, thorium. Rejection of these impurities can simplify downstream processing. The presence of iron minerals in a monazite concentrate would have the same beneficial effect.

The effect of the iron minerals on the monazite acid bake was strongly dependent on bake temperature and could be divided into four main temperature ranges. Bake temperatures of 200–250 °C were characterised by high dissolution of rare earths as well as impurities such as phosphate, thorium and iron, due to reactions of monazite and iron minerals with acid to form soluble sulfates. After baking at 400–500 °C, the leaching of phosphorus, iron and thorium decreased due to formation of an ill-defined, amorphous, insoluble iron sulfate-polyphosphate type phase. At 650 °C, the iron sulfate-polyphosphate type phase was altered to a more soluble form leading to an increase in the dissolution of phosphorus and the iron associated with the polyphosphate type phase. This process may have been initiated by the decomposition of ferric sulfate. After baking at 800 °C, ferric sulfate had decomposed and a mixture of crystalline $FePO_4$ and Fe_2O_3 had formed. Monazite, CeO_2 and the mixed oxide $Ce_{0.5}Th_{0.5}O_2$ were also formed, depending on the iron mineral. For acid baking of goethite and magnetite with monazite, the formation of these phases led to a significant decrease in the leaching of thorium, rare earth elements and iron.

CRediT authorship contribution statement

John Demol: Methodology, Investigation, Data curation, Writing – original draft, Writing – review & editing. **Elizabeth Ho:** Methodology, Supervision, Writing – review & editing. **Karin Soldenhoff:** Conceptualization, Resources, Writing – review & editing. **Inna Karatchevtseva:** Formal analysis. **Gamini Senanayake:** Supervision, Funding acquisition, Writing – review & editing.

Declaration of Competing Interest

The authors declare that they have no known competing financial interests or personal relationships that could have appeared to influence the work reported in this paper.

Acknowledgements

The authors would like to thank the following ANSTO scientists and personnel: Brian Young and Kathryn Prince for assistance with QEMSCAN analyses, Chris Griffith for assistance with TG-DSC analyses, the analytical team at ANSTO Minerals for providing ICP-OES, ICP-MS and XRF analyses and Gordon Thorogood for assistance with XRD analyses. This work was funded by an Australian Government Research Training Program (RTP) scholarship to John Demol for PhD research through Murdoch University and by ANSTO Minerals and carried out at ANSTO.

Appendix A

Table 12
Thermodynamic data for species identified in this work and related species or constituents.

Species[a]	$\Delta_f H°$	$S°$	$\Delta_f G°$
	kJ mol^{-1}	J mol^{-1} K^{-1}	kJ mol^{-1}
$H_2SO_4(l)$	−814	156.899	−689.925
$H_2SO_4(g)$	−735.13	298.799	−653.363
$SO_3(g)$	−395.764	256.772	−371.011
$SO_2(g)$	−296.812	248.22	−300.092
$O_2(g)$	0	205.149	0
$H_3PO_4(l)$	−1278.999	110.499	−1118.918
$H_2O(g)$	−241.826	188.832	−228.581
$Fe_2(SO_4)_3$	−2585.2	305.6	−2264.371
$FeSO_4$	−928.848	120.959	−824.886
$FePO_4$	−1296.998	93.721	−1182.224

(*continued on next page*)

Table 12 (*continued*)

Species[a]	$\Delta_f H°$	$S°$	$\Delta_f G°$
	kJ mol^{-1}	J mol^{-1} K^{-1}	kJ mol^{-1}
Fe_2O_3	−824.781	87.4	−742.825
FeOOH	−561.5	59.7	−490.519
Fe_3O_4	−1115.5	146.147	−1012.343
$LaPO_4$	−1969.599	108.239	−1850.323
$La_2(SO_4)_3$	−3932	319	−3597.502
H_3PO_4	−1278.999	110.499	−1118.918
$Th_3(PO_4)_4$[b]	−7154.64	429	−6695
$Th(SO_4)_2$	−2542.6	159	−2310.778

Data from (a) HSC Chemistry, Version 8.0 and (b) Bickel and Wedemeyer (1993).

Appendix B

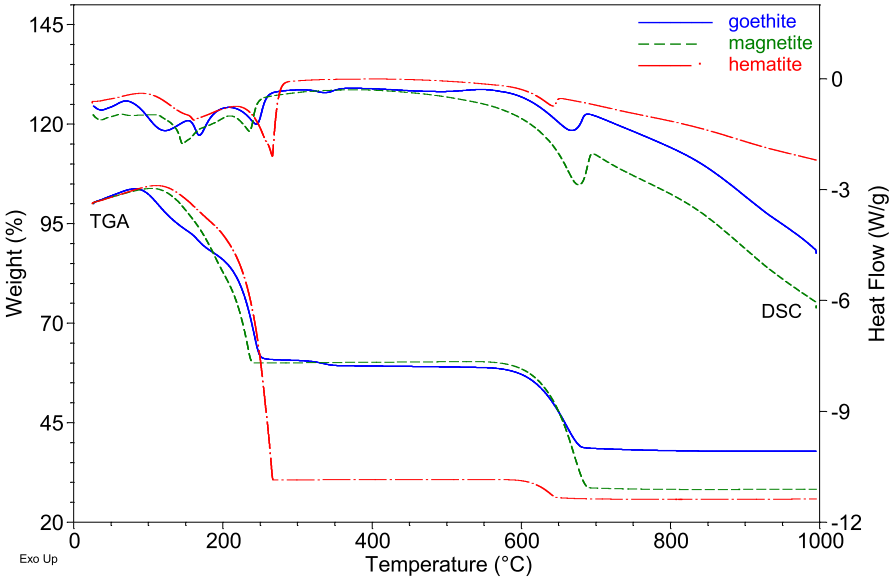

Fig. 16. TG and DSC curves for mixtures of sulfuric acid with hematite, goethite and magnetite samples (5 °C/min, under air)

Appendix C

C.1. Example elemental mass balance

Table 13
Elemental mass balance for acid baking and leaching of goethite with monazite (1:1 w/w) at 500 °C.

	Monazite+ goethite (1:1 w/w)	Baked solids	Leach residue	Leach filtrate	Wash filtrate	Accountability
Mass (g)	20.00	30.42	18.92	1176	233.1	
Elemental deportment						
Element*	mg	mg	mg	mg	mg	%
Fe	3022	2818	2505	319	42	95
P	921	902	769	107	6	96
Th	461	440	199	212	10	91
Ce	1795	2875	118	1551	26	94
La	926	1487	59	826	14	97
Nd	717	1205	59	633	10	98
Pr	181	179	13	166	3	100
TRE**	3874	3730	308	3367	57	96

* Fe and Th in solids were analysed by XRF; P in solids was analysed by digestion and ICP-OES analysis of the digest solution. Fe and P in solutions were analysed by ICP-OES; Th in solutions was analysed by ICP-MS.
** Total rare earths.

C.2. Extraction calculations

The extent of elemental dissolution during leaching after baking was calculated by comparing the mass of an element in either the final solid residue, or the final leach solution, to the mass of that element in the starting material(s). For elements where the dissolution was high, the degree of dissolution was based on the final solid residue and feed assay, according to Equation (a) below. For elements where the dissolution was low, the

degree of dissolution was based on the final leach solution and feed assay, according to Equation (b). For sulfur, the starting material was considered to be the baked solid before leaching, to avoid including the sulfuric acid volatilised during the bake. The accountability for each element was also calculated to ensure that it was within the range of 90–110%.

(a) Dissolution (%) = $(M_{feed} - M_{residue})/M_{feed} * 100$
(b) Dissolution (%) = $M_{solution}/M_{feed} * 100$

Where:
M = element,
M_{feed} = mass of element in starting materials before baking,
$M_{residue}$ = mass of element in solid residue after baking and leaching, and
$M_{solution}$ = mass of element in final clarified leach liquor.

C.3. Dissolution of Individual Light Rare Earths

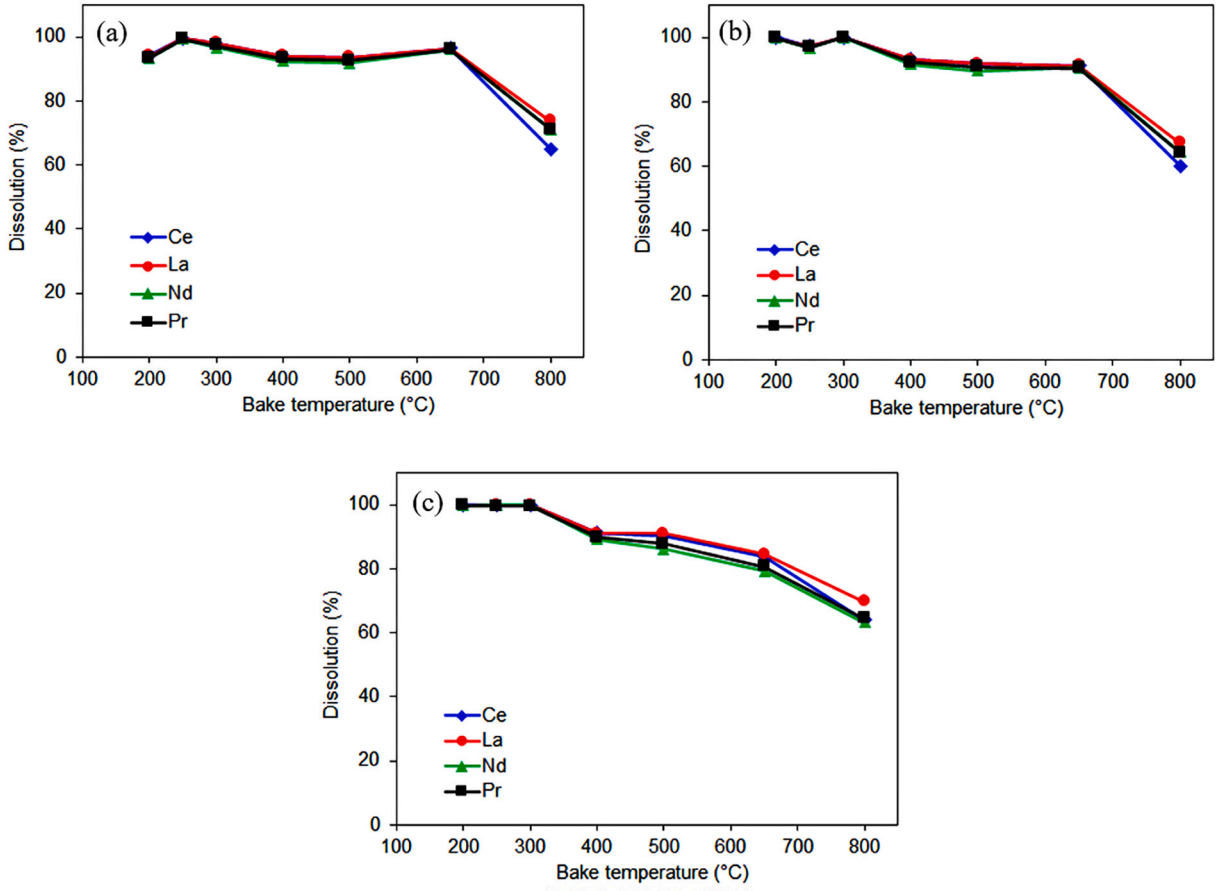

Fig. 17. Individual light rare earth dissolution during leaching in 0.9 M H_2SO_4 after acid bakes of 1:1 (*w*/w) mixtures of (a) monazite/goethite, (b) monazite/magnetite and (c) monazite/hematite samples relevant to Fig. 2.

References

Bickel, Michael, Wedemeyer, Horst, 1993. Th Thorium Supplement Volume C 8 Compounds wtih Si, P, As, Sb, Bi, and Ge, 8th. In: Keim, Rudolf, et al. (Eds.), Gmelin Handbook of Inorganic and Organometallic Chemistry. Springer, Berlin.

Bingham, P.A., Hand, R.J., 2008. Sulphate incorporation and glass formation in phosphate systems for nuclear and toxic waste immobilization. Mater. Res. Bull. 43 (7), 1679–1693.

Castor, S.B., Hedrick, J.B., 2006. Rare earth elements. In: Kogel, J.E., Tivedi, N.C., Barker, J.M., Krukowski, S.T. (Eds.), Industrial Minerals and Rocks – Commodities, Markets and Uses. 7th edition. Society for Mining, Metallurgy, and Exploration, Littleton, Colorado, pp. 769–792.

Da, N., Grassmé, O., Nielsen, K.H., Peters, G., Wondraczek, L., 2011. Formation and structure of ionic (Na, Zn) sulfophosphate glasses. J. Non-Cryst. Solids 357 (10), 2202–2206.

Dacheux, N., Clavier, N., Wallez, G., Brandel, V., Emery, J., Quarton, M., Genet, M., 2005. Characterization of the thorium phosphate-hydrogenphosphate hydrate (TPHPH) and study of its transformation into the thorium phosphate-diphosphate (β-TPD). Mater. Res. Bull. 40 (12), 2225–2242.

Demol, J., Ho, E., Senanayake, G., 2018. Sulfuric acid baking and leaching of rare earth elements, thorium and phosphate from a monazite concentrate: effect of bake temperature from 200 to 800 °C. Hydrometallurgy 179, 254–267.

Demol, J., Ho, E., Soldenhoff, K., Senanayake, G., 2019. The sulfuric acid bake and leach route for processing of rare earth ores and concentrates: a review. Hydrometallurgy 188, 123–139.

Frost, R.L., Theiss, F.L., López, A., Scholz, R., 2014. Vibrational spectroscopic study of the sulphate mineral glaucocerinite $(Zn,Cu)_{10}Al_6(SO_4)_3(OH)_{32}·18H_2O$ – A natural layered double hydroxide. Spectrochim. Acta A Mol. Biomol. Spectrosc. 127, 349–354.

Gontijo, V.L., Teixeira, L.A.V., Ciminelli, V.S.T., 2020. The reactivity of iron oxides and hydroxide during low-temperature sulfation. Hydrometallurgy 197, 105452.

Kim, E., Osseo-Asare, K., 2012. Aqueous stability of thorium and rare earth metals in monazite hydrometallurgy: Eh–pH diagrams for the systems Th–, Ce–, La–, Nd–(PO4)–(SO4)–H2O at 25°C. Hydrometallurgy 113–114, 67–78.

Li, H., Zhao, N., Zhang, G., Liu, Y., Long, Z. and Huang, X., 2009. A process of smelting monazite rare earth ore rich in Fe. Australian Patent No. AU 2008286599. Grirem Advanced Materials Co., Ltd.

Lucas, J., Lucas, P., Le Mercier, T., Rollat, A., Davenport, W.G., 2015. Rare Earths: Science, Technology, Production and Use. Elsevier, Amsterdam.

Lynas Corporation Ltd, 2011. Roskill International Rare Earths Conference Presentation, 7th International Rare Earths Conference, Hong Kong.

Mackowski, R., Raiter, R., Soldenhoff, K. and Ho, E., 2009. Recovery of Rare Earth Elements. Australian Patent No. AU 2008201945. Arafura Resources Ltd.

Möncke, D., Sirotkin, S., Stavrou, E., Kamitsos, E.I., Wondraczek, L., 2014. Partitioning and structural role of Mn and Fe ions in ionic sulfophosphate glasses. J. Chem. Phys. 141 (22), 224509.

Mu, J., Perlmutter, D.D., 1981. Thermal decomposition of inorganic sulfates and their hydrates. Ind. Eng. Chem. Process Des. Dev. 20 (4), 640–646.

Newbury E., Dale, Ritchie W.M., Nicholas, 2013. Is scanning electron microscopy/energy dispersive X-ray spectrometry (SEM/EDS) quantitatve? Scanning 35, 141–168.

Newbury E., Dale, Swyt R., Carol, Myklebust L., Robert, 1995. "Standardless" quantitative electron probe microanalysis with energy-dispersive X-ray spectrometry: is it worth the risk? Anal. Chem. 67, 1866–1871.

Schwartz, D., Gadiou, R., Brilhac, J.-F., Prado, G., Martinez, G., 2000. A kinetic study of the decomposition of spent sulfuric acids at high temperature. Ind. Eng. Chem. Res. 39 (7), 2183–2189.

Siriwardane, R.V., Poston Jr., J.A., Fisher, E.P., Shen, M.S., Miltz, A.L., 1999. Decomposition of the sulfates of copper, iron(II), iron(III), nickel and zinc: XPS, SEM, DRIFTS, XRD and TGA study. Appl. Surf. Sci. 152, 219–236.

Socrates, G., 2001. Infrared and Raman Characteristic Group Frequencies: Tables and Charts. John Wiley and Sons, Chichester.

Soltani, F., Abdollahy, M., Petersen, J., Ram, R., Becker, M., Javad Kholeini, S.M., Moradkhani, D., 2018. Leaching and recovery of phosphate and rare earth elements from an iron-rich fluorapatite concentrate: part I: direct baking of the concentrate. Hydrometallurgy 177, 66–78.

Tagawa, H., 1984. Thermal decomposition temperatures of metal sulfates. Thermochim. Acta 80 (1), 23–33.

Teixeira, L.A.V. and Silva, R.G., 2015. System and process for selective rare earth extraction with sulphur recovery. U.S. Patent No. US 2015/0329940. VALE S.A., United States.

Wall, F., 2014. Rare earth elements. In: Gunn, G. (Ed.), Critical Metals Handbook. John Wiley & Sons, pp. 312–339.

Wang, X.Y., Liu, J.M., Li, M., Fan, H.L., Yang, Q.S., 2010. Decomposition reaction kinetics of Baotou RE concentrate with concentrated sulfuric acid at low temperature. Rare Metals 29 (2), 121–125.

Yoon, H.S., Kim, C.J., Chung, K.W., Jeon, S., Park, I., Yoo, K., Jha, M.K., 2015. The effect of grinding and roasting conditions on the selective leaching of Nd and Dy from NdFeB magnet scraps. Metals 5, 1306–1314.

Zhang, Z., Jia, Q., Liao, W., 2015. Chapter 277 - Progress in the separation processes for rare earth resources. In: Jean-Claude, B., Vitalij, K.P. (Eds.), Handbook on the Physics and Chemistry of Rare Earths. Elsevier, North Holland, pp. 287–376.